Rinta-Paavola, Aleksi; Sukhomlinov, Dmitry; Hostikka, Simo

Modelling Charring and Burning of Spruce and Pine Woods During Pyrolysis, Smoldering and Flaming

Published in:
Fire Technology

DOI:
10.1007/s10694-023-01458-9

Published: 01/09/2023

Document Version
Publisher's PDF, also known as Version of record

Fire Technology, 59, 2751–2786, 2023

Manufactured in The United States
https://doi.org/10.1007/s10694-023-01458-9

Modelling Charring and Burning of Spruce and Pine Woods During Pyrolysis, Smoldering and Flaming

Aleksi Rinta-Paavola, *Department of Civil Engineering, Aalto University, Rakentajanaukio 4, 02150 Espoo, Finland*
Dmitry Sukhomlinov, *Department of Chemical and Metallurgical Engineering, Aalto University, Kemistintie 1, 02150 Espoo, Finland*
*Simo Hostikka**, *Department of Civil Engineering, Aalto University, Rakentajanaukio 4, 02150 Espoo, Finland*

Received: 12 December 2022/**Accepted:** 21 June 2023/**Published online:** 1 July 2023

Abstract. The goal of this work is to develop a material model for Norway spruce and Scots pine woods for use in performance-based fire safety design to predict char front progress and heat release in burning timber. For both woods a set of two different models is estimated: one that assumes wood as a single component and another that considers the pyrolysis of wood principal components independently (single and parallel reactions models, respectively). The material models are calibrated using cone calorimeter experiments. The models are intended for a number of different fire scenarios, such as fully developed fire with only little oxygen in the compartment, or the decay period after flaming with exposed char still smoldering. For both spruce and pine, the single and parallel reactions models are able to predict the experiments in the scale of cone calorimeter with near-equal accuracy. Hence, the single reaction model emerges as the preferable level of complexity when modelling charring and heat release, avoiding the increased uncertainty associated with the additional parameters of the parallel reactions model. When scaling up to the simulations of large scale fire tests, the models can predict the char front progress, but the final temperature profile differs from the experimental. The effects of crack forming in the char layer is one of the likely causes, but its mechanisms are not sufficiently known. Therefore, we suggest a closer study on crack formation in wood under fire as future research.

Keywords: Charring, Cone calorimeter, Pine wood, Pyrolysis, Smoldering, Spruce wood

1. Introduction

In recent times, there has been a considerable rise in interest to timber construction, increasingly in tall buildings as well. Timber as a construction material has an inherent fire risk, and the verification of fire safety of timber buildings, espe-

*Correspondence should be addressed to: Simo Hostikka, E-mail: simo.hostikka@aalto.fi

cially tall ones, require sophisticated modelling tools. Charring of timber during fire is a complex process. In fire safety engineering, it is modeled by a thermal, or material, model for a solid phase. Meanwhile, heat release and temperature in the gaseous phase are modeled by a fire model [1], which acts as a boundary condition for the thermal model and as a driving force for wood pyrolysis and charring. Current research on fire testing of massive timber compartments shows, that unprotected structural timber components have significant contribution to the total heat release. Regarding the behavior of the timber material itself, significant knowledge gaps are identified within self-extinguishment of the flaming combustion and smoldering during the post-flaming decay phase [2–4]. A successful material model for use in modern timber buildings should be able to account for all these three phenomena. When modelling material response to fire, one has to choose a suitable level of complexity for the thermal model. Even though the increasing computational power allows more and more complex models, a persisting problem is any new model parameter increasing the model uncertainty [5].

To satisfy different purposes, literature has an extensive variety of models to describe char propagation in timber. The simplest possible model is a constant charring rate, for example as provided in Eurocode 5, Part 1–2 [6]. It is extremely easy to apply, but it comes with severe limitations. The constant charring rate is based on the standard temperature curve, which itself offers an unrealistic fire scenario, lacking any cooling phase and dependence on ventilation conditions or fire load. To counter this, Eurocode also provides a method to determine a parametric fire and a corresponding charring rate as a function of aforementioned factors [6, 7]. However, the parametric fire has also its limitations. It is applicable only to certain compartment sizes and ventilation conditions and does not necessarily give an accurate prediction of temperature even in a compartment that meets the criteria. Hakkarainen [8] found out in the performed compartment fire tests, that the temperature prediction by the Eurocode parametric fire curve is overtly conservative especially for tests with exposed timber boundaries contributing to the fire load. Salminen [9] further confirmed that the char depth calculated by the parametric method corresponding to experimental conditions in [8] was overtly conservative.

Various empirical models for char propagation have been proposed in literature based on a range of different experimental data. The purpose of these models is to better relate the char propagation to actual fire conditions in the gaseous phase. For example, Mikkola [10] presents an empirical model for charring rate in timber as a function of wood density, moisture content and external heat flux. The model is based on experiments under a cone calorimeter. Babrauskas [11] presents his own model for charring under a cone calorimeter based on review of earlier published works. Contrary to the linear charring rate under a constant exposure in the model of Mikkola [10], charring rate decreases over time in the model of Babrauskas [11]. It is widely accepted that a char layer forms a protective barrier that delays further decomposition inside the wood. In addition to the heat flux and wood density dependence, the charring rate in the model of Babrauskas [11] includes a rough correction for reduced oxygen content. Lau et al. [12] present an empirical charring model and review some existing correlations for char propaga-

tion in timber, for many of which the gaseous phase boundary condition is ASTM E 119, a standard fire similar to ISO 834. Not even the qualitative behavior was consistent with all of the correlations, as some of them produce decreasing and some even increasing charring rates over the same ASTM E 119 fire exposure. This represents a drawback of empirical models, as they are inherently dependent on the experimental configuration in which they are determined, and could not be generalized to all scenarios.

Eurocode 5 [6] allows for "advanced calculation methods" in fire design to be applied in determination of char depth, development of temperature profile within structural members and in evaluation of structural behavior. It however does not specify exactly the numerical methodology. Both in research literature and in practical applications finite element methods (FEM) are the dominant choice. SAFIR [13] is an example of FEM software widely used in structural fire modelling in general, applied also for timber. Effects of chemical reactions are not taken into account explicitly, but rather indirectly as effective thermal properties. The effective thermal properties of Eurocode 5 [6] are valid only for the ISO 834 standard fire exposure. As a response, effective thermal properties to account for woods of different moisture contents, densities and heating conditions have been developed [14, 15]. As a further improvement, Pečenko et al. [16–18] have presented a finite element model to analyse charring and mechanical behavior of charring wood where moisture transport is modeled separately. This approach allows for modelling of multiple scenarios with a single set of thermal properties as the effect of moisture needs not to be included in their effective values. Most recently, they have expanded their model by inclusion of wood pyrolysis [19].

Models for char propagation based on heat transfer and chemical kinetics of pyrolysis have been presented in the research literature. Some of the early examples of numerical wood pyrolysis models are works of Kung [20] and Atreya [21], in both of which wood decomposition is controlled by a first-order Arrhenius-type reaction. Kung [20] presents a model that gives temperature and conversion profiles and mass loss rate in pyrolyzing wood, but it is not experimentally validated, and he admits several model parameters being rough estimations. The model developed by Atreya [21] focuses on prediction of flame spread on horizontal surfaces. Moghtaderi et al. [22] and Spearpoint and Quintiere [23] present examples of a model combining chemistry and heat transfer in different species of wood and thermoplastics under a cone calorimeter. These models however are greatly simplified, as for example the pyrolysis rate of solid is controlled only by the heat of reaction. In the work of Lautenberger et al. [24] the pyrolysis rate is controlled by the Arrhenian kinetic equation. However, charring still proceeds as an infinitely thin front. The model is calibrated using mass loss and specimen surface temperature measured in a cone calorimeter. In a later work, Lautenberger and Fernandez-Pello [25] present a more complex model, where the material thermal properties and kinetic parameters are similarly obtained by model fitting to experimental data from irradiated wood specimen. The more detailed reaction model in their work allows thermal decomposition across the solid, the reaction rate being controlled by temperature, including oxidation as a competing reaction to non-oxidative pyrolysis. In addition, diffusive transport of oxygen and released decompo-

sition products and water vapor are modeled. As an example of a more recent work, Richter and Rein [26] have developed a detailed model for charring of timber, that considers independent decomposition of wood primary components of hemicellulose, cellulose and lignin through pyrolysis and oxidation, though lignin decomposing only via pyrolysis. Using the same model, they provide a rare example of applying a detailed material model in the prediction of charring of large scale timber specimens, studying the response to various design fires [27].

Char layer acts as a natural barrier against further decomposition deeper inside the flaming timber member, but the shielding effect is compromised, as cracks allow easy passage for heat and oxygen inside the wood [28, 29], or as the char layer is consumed by oxidation [30]. Hence, understanding and modelling these phenomena are important for predictions of char front progress. However, Li et al. [28] stated in 2017 the cracking of char to be ''beyond the capabilities of the current modelling techniques'', which as of now is still the status with Fire Dynamics Simulator [31], one of the foremost modelling tools within the fire community. Richter et al. [30] have recently presented a detailed experimental and computational study on charring and oxidation of particleboard under different conditions. They established the heat flux and ambient oxygen concentration as the main parameters controlling the charring rate and the burning mode between pyrolysis, smoldering and flaming. Cross-laminated timber is one of the most important wood products used in massive timber construction, but its charring under fire often leads to delamination of charred layers, revealing unexposed virgin surface.

The purpose of this work is to create numerical material models for spruce and pine timbers for estimating char front progress in fire-related computational fluid dynamics simulations. These are the main structural timbers used in the Nordic countries, but there exists no pyrolysis model designed specifically for them, that would also account for oxidation. The numerical models are based on heat transfer and chemical kinetics, thus the conversion from wood to char is controlled by the surrounding fire conditions. Experimental cone calorimeter test data in non-oxidative nitrogen atmosphere, in smoldering conditions in standard atmosphere, and in flaming conditions in standard atmosphere are used in model estimation. We utilize the kinetics for oxygen-independent pyrolysis determined in [32]. The chemical kinetics for surface oxidation of char is evaluated using cone calorimeter tests in standard atmosphere, both in smoldering and flaming conditions, and the material thermophysical properties are adjusted to satisfy the cone calorimeter tests across all experimental conditions. This is for model validity in multiple different fire scenarios, such as flashover, where oxygen concentration in the burning compartment is near-zero, or in the decay phase after flaming combustion, where hot charred wood is in contact with air. Finally, the models are tested in reproducing the observed char front propagation in large scale fire tests.

Table 1
Primary Component Composition by Weight Percentage [33], and the Dry Densities of Spruce and Pine Woods [32]

Species	Extractives	Hemi-cellulose	Cellulose	Lignin	Residual	Dry density (kg/m^3)
Picea abies	1.7	28.3	41.7	27.4	0.9	408
Pinus sylvestris	3.5	28.5	40.0	27.7	0.3	493

2. Materials and Methods

2.1. Wood Materials

The experiments were carried out using samples of Norway spruce (*Picea abies*) and Scots pine (*Pinus sylvestris*) woods. We assume dry densities of spruce and pine of 408 and 493 kg/m^3, respectively, as measured in [32]. Their reported variations were 342 kg/m^3 to 441 kg/m^3 and 467 kg/m^3 to 529 kg/m^3, respectively, except for a few pine samples with very high apparent heartwood fraction that had a density of approximately 600 kg/m^3. In this research, the samples were conditioned at 20°C and 45% relative humidity, leading to a moisture content of $9.0 \pm 0.75\%$ for both species on wet basis. Table 1 presents the primary component compositions for both species according to [33], which were assumed to hold in this work. The table also reports dry densities of the woods [32].

2.2. Experimental

The main experimental method in this research is cone calorimetry. The cone calorimeter employed in this research is manufactured by Concept Equipment, and it could be operated as a standard cone calorimeter conforming to the ISO 5660-1 standard, or as a controlled atmosphere cone calorimeter. The latter mode is enabled by sealing the sides and the top of the testing compartment and feeding in nitrogen and compressed air in a desired ratio. The specimen may be brought into near-zero oxygen atmosphere, when flushing only with nitrogen.

Spruce and pine specimens of 2 cm in thickness and 10 by 10 cm in exposed cross section were tested in horizontal operation under near oxygen-free atmosphere, and in smoldering and flaming conditions, the latter two being under ambient atmosphere. Each experiment is replicated three times, and any representation of a cone calorimeter test in this paper is the experimental average or their variation. At all tests, specimen was wrapped in aluminum foil on all nonexposed sides and placed on a 1.3 cm layer of ceramic wool, the direction of heat flux being in perpendicular to the grain. During the near oxygen-free operation the sealed testing compartment was flushed with a nitrogen flow of 4 l/s, while the cone calorimeter exhaust fan was set at 8 l/s, the difference being made up of surrounding air entering between the bottom of the exhaust hood and the top of the testing compartment. The smoldering conditions were established by means of absence of pilot ignition spark and using sufficiently low heat flux levels to avoid

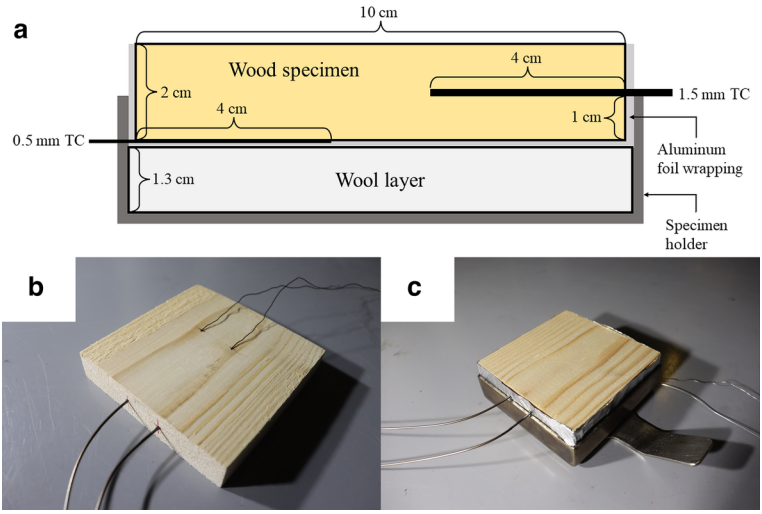

Figure 1. (a) Side view of thermocouple (TC) placement inside the specimen. The exposed surface is at the top. (b) Instrumented cone calorimeter specimen. The specimen is upside down compared to the orientation during the experiment, the exposed surface being here at the bottom. (c) Instrumented cone calorimeter specimen wrapped from the sides and back in aluminum foil inside a sample holder, ready for testing.

autoignition. Pyrolysis experiments were carried out under heat flux levels of 35 and 50 kW/m^2 for both woods, smoldering experiments under 25 and 35 kW/m^2 for spruce and 20 and 30 kW/m^2 for pine, as it was found out to self-ignite at 35 kW/m^2. Flaming experiments were carried out at 25, 35 and 50 kW/m^2 for both woods. Pyrolysis and flaming experiments under 35 kW/m^2 were replicated with installed thermocouples at halfway inside the specimen (1 cm depth) and at its unexposed surface (2 cm depth), two sensors for each depth. This had to be done separately from the experiments measuring mass loss, as thermocouple wires caused tension to the sample. Looking from above, the temperature measurement points were positioned at the corners of a 2 cm square, centered on the middle of the specimen. All thermocouples were of K-type (estimated uncertainty of $\pm$ 2.5°C in ambient, $\pm$ 5.3°C in the highest measured temperatures of approximately 700°C). Those installed inside the specimen were inserted horizontally in perpendicular to the heat flow and were 1.5 mm in diameter, tightly fitting into the drilled hole, and those on the unexposed surface were 0.5 mm in diameter, positioned between the wood specimen and the foil wrapping. Figure 1 presents a side view of thermocouple positioning and photographs of an instrumented specimen, showing the thermocouple positioning on the unexposed side, and the assembled specimen inside the holder. In the finished specimen assembly, thermocouples would be punctured through the foil wrapping, and the specimen was laid carefully on the ceramic wool layer, so that the thermocouples in between would stay stationary.

We acknowledge the uncertainty in the thermocouple position at 1 cm depth, associated with drilling a long horizontal hole for the thermocouple. Our first approach was to drill a tight-fitting hole for 0.5 mm thermocouple from the unexposed side to 1 cm depth. However, these results proved unacceptable, as the thermocouple wire was conducting an excessive amount of heat away from the measuring point, even though it was the narrowest that could be practically used for the purpose.

The thermal diffusivities of spruce and pine woods were measured with the laser flash analysis (LFA) method. The measurements were conducted with Netzsch LFA 427 apparatus equipped with an S-type sample thermocouple (estimated uncertainty of $\pm$ 1°C) and an InSb IR detector. The measurements were performed in a nitrogen atmosphere (50 mL/min flowrate, 99.999 vol% pure). The laser voltage applied was 650 V with 0.5 ms pulse width. For the measurements the wood samples were machined into a shape of a flat cylinder 12.4 mm to 12.7 mm in diameter and 2.90 mm to 4.25 mm thick. The samples were prepared in such a way that the thermal diffusivity was measured in the direction perpendicular to the grain. Both sides of the samples were coated with a graphite spray prior to the measurements. Three identical measurements were performed at each temperature within the range of 20°C to 200°C with 20°C steps. The generated raw data were post processed with the Standard model by Netzsch, which is an improved Cape and Lehman model [34].

Wood shrinkage at cellular level was studied using scanning electron microscope (SEM) pictures of spruce wood. The SEM specimen was a cube with approximately 5 mm edges. The specimen was smoothed by soaking overnight in distilled water before cutting the pictured surface in perpendicular to the grain with a razorblade, to reveal a clean-cut surface. The cut specimen is dried overnight at 100°C.

The micrographs were captured with FEI Quanta FEG 450 scanning electron microscope, using backscattered electron detector and a beam voltage of 7 kV to 10 kV, adjusted individually for each micrograph. The micrographs were taken in the low-vacuum mode (60 Pa H_2O vapor) without conductive coating on the specimen. The reference SEM image of the spruce specimen was taken before any thermal treatment directly after the overnight drying at 100°C. To study the surface of wood pyrolyzed at different temperatures, the same specimen was subjected to heating steps in the furnace of DuPont Instruments 951 thermogravimetric analyzer under helium flow. Firstly, the specimen was brought with a rate of 5°C/min from ambient to 250°C where it was kept for 10 min, and allowed to cool to ambient before opening the furnace and removing the specimen. After this treatment, a SEM image was taken from the exact same location of the specimen as the reference image. At the next heating step, the same specimen was first heated with 20°C/min to the previous maximum temperature of 250°C, then with 5°C/min to 325°C, where it was again kept for 10 min and let to cool to ambient, finally taking a SEM image at the same location as the previous ones. This was repeated with the maximum temperatures of 400, 475 and 550°C, bringing the sample with 20°C/min to the previous maximum temperature, and

$$
a\begin{cases} wood \rightarrow char + volatiles \\ char \xrightarrow[+O_2]{} CO_2 \\ water \rightarrow water\ vapor \end{cases}
$$

$$
b\begin{cases} hemicellulose \rightarrow char + volatiles \\ cellulose \rightarrow char + volatiles \\ lignin \rightarrow char + volatiles \\ char \xrightarrow[+O_2]{} CO_2 \\ water \rightarrow water\ vapor \end{cases}
$$

Figure 2. Reaction schemes employed in this work: (a) single reaction, (b) parallel reactions.

subsequently with 5°C/min to the new maximum temperature, taking SEM images after each heating step.

2.3. Reaction Schemes

This work uses the same reaction schemes as employed by Rinta-Paavola and Hostikka [32], namely the single reaction and parallel reactions schemes, now expanded with char oxidation. The single reaction scheme assumes a homogenous virgin material which decomposes into char and volatiles through pyrolysis reaction. The parallel reactions scheme instead assumes each of the wood main components (hemicellulose, cellulose and lignin) pyrolyzing through independent reactions. Rinta-Paavola and Hostikka [32] concluded that in a macroscopic model, extractives have negligible effect, even though in a model for microscale experiments (e.g. thermogravimetry) they could be essential. Therefore, in this work extractives are combined to hemicellulose.

The conclusion of the work of Rinta-Paavola and Hostikka [32] was that both models, either the single or parallel reactions one, can reproduce the experimentally measured heat release in cone calorimeter with near-equal performance. Their measurements however were integral in nature, measuring only the heat release and mass loss over the whole specimen. The more detailed measurements in this research aim to give more comprehensive answer on the optimal level of reaction scheme complexity in predicting the temperature profile development inside a charring wood specimen, a question not answered in the literature specifically for the studied species of wood. Another justification for carrying over both reaction schemes from the previous work [32] are the findings of Adibaskoro et al. [35], that show the degradation of strength and pyrolysis shrinkage in spruce wood to coincide with hemicellulose and cellulose pyrolysis, respectively. Hence, the parallel reactions scheme may be useful in prediction of pre-charring strength loss of timber in further research.

Figure 2 shows the reaction schemes employed in this work (single and parallel reactions, a and b, respectively). Our initial study revealed that an oxidation reaction for virgin wood does not improve the quality of the model, so char oxidation

was maintained as the only oxygen-dependent reaction. Moisture evaporation (bound water to water vapor) is considered as its own reaction.

2.4. Numerical

Numerical pyrolysis simulations were carried out using the condensed phase pyrolysis solver of Fire Dynamics Simulator (FDS) version 6.7.7 [36, 37]. FDS is a computational fluid dynamics model, meant to numerically solve Navier–Stokes equations for low Mach number flows driven by fire, modelling turbulence by Large Eddy Simulation. It contains a model for heat transfer and pyrolysis in solids. The detailed mathematical model is found in [37].

The reaction rate at the depth x is determined by Arrhenian kinetics.

$$r_\alpha(x) = \left(\frac{\rho_{s,\alpha}(x)}{\rho_{s,0}}\right)^{n_\alpha} A_\alpha \exp\left(-\frac{\mathrm{E}_\alpha}{\mathrm{RT_s(x)}}\right) \mathrm{X}_{\mathrm{O_2}}^{\mathrm{n_{O_2,\alpha}}} \tag{1}$$

where $\rho_{s,\alpha}$ is the mass concentration of component α, $\rho_{s,0}$ is the initial density of the solid material layer, n_α is the reaction order, A_α is the pre-exponential factor, E_α is the activation energy, R is universal gas constant, T_s is the solid temperature at depth x, $X_{\mathrm{O_2}}$ is the local oxygen volume fraction inside the solid, and $n_{\mathrm{O_2},\alpha}$ is the reaction order with respect to oxygen.

The reader should note, from FDS version 6.7.8 onwards the mass concentration term in Equation 1 takes the form $\rho_{s,\alpha}(x)^{n_\alpha}$ by rejecting $\rho_{s,0}$ in denominator. If the reaction order is equal to unity, kinetic parameters may be carried out unchanged between the old and new versions of FDS. If $n_\alpha \neq 1$, reaction rates between the old and current versions of FDS could be brought to agreement by adjusting the pre-exponential factor according to Equation 2 [31].

$$A_{\alpha,\mathrm{new}} = \frac{A_{\alpha,\mathrm{old}}}{{\rho_{s,0}}^{n_\alpha - 1}} \tag{2}$$

where $A_{\alpha,\mathrm{new}}$ and $A_{\alpha,\mathrm{old}}$ are the pre-exponential factors in FDS versions 6.7.8 or later and 6.7.7 or earlier, respectively.

The model does not solve for the mass transfer processes. Instead, we assume that the oxygen volume fraction at a depth x follows an exponential decay from the gaseous phase value $X_{\mathrm{O_2},g}$ next to the solid.

$$X_{\mathrm{O_2}}(x) = X_{\mathrm{O_2},g} \exp\left(-\mathrm{x}/\mathrm{L_g}\right) \tag{3}$$

where L_g is the gas diffusion length scale following from the competing diffusion and reactive consumption.

FDS solves heat transfer in solid phase according to one-dimensional heat equation.

$$\rho_s c_s \frac{\partial T_s}{\partial t} = \frac{\partial}{\partial x}\left(k_s \frac{\partial T_s}{\partial x}\right) + \dot{q}_s''' \tag{4}$$

where c_s is the specific heat capacity of the material mixture, t is time and k_s is the thermal conductivity of the solid material mixture. The chemical source term $\dot{q}_s'''$ represents the release or binding of energy by exo-, and endothermic reactions, respectively.

PROPTI [38] is employed as the parameter estimation tool. Over the course of estimation, PROPTI executes the model using the linked fire simulation software (here FDS), passes the simulation results to the optimizer, which in turn decides if further evaluations are necessary. PROPTI by default uses SPOTPY optimization package [39]. The employed estimation method in this work is shuffled complex evolution.

3. Results and Discussion

3.1. Parameter Estimation Procedure

Our initial strategy for model estimation was as follows: firstly, to estimate kinetic parameters for water evaporation, heats of pyrolysis and char emissivity from oxygen-free cone calorimeter tests under 35 kW/m^2, assuming wood pyrolysis kinetics determined in [32]; then maintaining the previously estimated parameters, to estimate char oxidation kinetic parameters from smoldering cone calorimeter experiments under 35 or 30 kW/m^2 (spruce and pine, respectively); finally using the other tests under different heat fluxes and those in flaming conditions as model validation. The water evaporation kinetics were estimated using current results from cone calorimeter experiments, because our preliminary simulations revealed, that those estimated to thermogravimetric results in [32] were not able to reproduce the experimental temperature development inside the specimen. This strategy worked out well for the single reaction spruce model, but for the parallel reactions spruce model and both of the pine models, the model fit to flaming experiments was unacceptable. Therefore, the parallel reactions model for spruce, and the single-, and parallel reactions models for pine were estimated using the experimental data in oxygen-free, smoldering and flaming conditions simultaneously as the target data. Experimental data under 35 kW/ m^2 was used for all different experimental conditions in the new estimation strategy as well, by exception of using experiment under 30 kW/m^2 for smoldering pine. After estimating the single reaction spruce model according to our initial strategy, to minimize the amount of estimated parameters, we assume the same water evaporation kinetic parameters and char emissivity to hold for all other models as well. Table 2 presents the estimated model parameters.

In the initial model estimations for the parallel reactions models, the lignin heat of pyrolysis converged near to the values estimated to differential scanning calorimetry experiments by Rinta-Paavola and Hostikka [32], − 1230 and − 1250 kJ/kg for spruce and pine, respectively. Heats of pyrolysis for lignin were

Table 2
Employed Model Parameters

	Single reaction scheme		Parallel reactions scheme	
Component, parameter	Spruce	Pine	Spruce	Pine
Water				
A (1/s)	8.37×10^{12}	8.37×10^{12}	8.37×10^{12}	8.37×10^{12}
E (kJ/mol)	121	121	121	121
n (–)	1	1	1	1
Wood				
H_r (kJ/kg)	112	140		
hc			249	404
c			253	629
l			− 1230	− 1250
ΔH_c (kJ/kg)	13,750	13,850		
hc			19,500	17,000
c			13,400	14,000
l			7000	7200
A (1/s)	4.691×10^{13} (2.121×10^{11}*)	2.007×10^{13} (7.724×10^{10}*)		
hc			5.426×10^{13} (6.065×10^{9}*)	3.194×10^{13} (9.49×10^{9}*)
c			4.239×10^{13} (4.25×10^{14}*)	2.146×10^{13} (2.453×10^{14}*)
l			2.46×10^{12} (8.491×10^{-2}*)	2.46×10^{12} (3.364×10^{-2}*)
E (kJ/mol)	190.5	185.1		
hc			168.1	168.1
c			195.1	191.2
l			157.5	157.5
n (–)	1.89	1.89		
hc			2.5	2.3
c			0.62	0.61
l			6.11	6.11
v_{char} (–)	0.16	0.16		
hc			0	0
c			0.043	0.033
l			0.517	0.517
Char				
ε (–)	0.838	0.838	0.838	0.838
ρ (kg/m^3)	52.5	104	20	72
n (–)	1	1	1	1
A (1/s)	3.75	1.79	23.5	3.18
E (kJ/mol)	27.7	27.7	32.5	32.5

Hemicellulose: *hc*; cellulose: *c*; lignin: *l*. Updated pre-exponential factors according to Equation 2 presented in parentheses where relevant and marked with an asterisk (*), calculated assuming an initial layer density when the moisture content is 9% by mass, wet basis

thus fixed to these values in the final estimations. To prevent the activation energy for pine char oxidation from converging to the minimum of any given estimation boundary, it was fixed for both single-, and parallel reactions models to the same value as estimated for the respective spruce model. Char density for each model, presented in Table 2, was estimated manually so that the final specimen thickness in an oxygen-free cone calorimeter simulation corresponds to that in the end of a cone calorimeter experiment in nitrogen, as FDS determines the final thickness by solid yield and the ratio of virgin and residue densities. With spruce, the specimen unexpectedly swelled by 12% on average from the initial thickness. Pine instead shrunk, as expected, by 28% on average from its initial state. For reference, Dupal et al. [40] estimated the bulk density of spruce char as 138 kg/m^3 on average, which is considerably more than our current estimated results. However, the spruce specimens in their work are significantly denser than in our work (average 508 kg/m^3, after minimum 24 h conditioning at 23°C and 50% relative humidity), and their opened charred specimens appear to have denser consistency than ours (Figure 22). Also, we treat char density in our model as an effective parameter instead, to have correct simulated final thickness of the specimen.

It is worth noting that the estimated char densities for the single-, and parallel reactions models are different. We believe this discrepancy is related to the different mechanisms of char production: the single reaction model produces char in a single step, and the conversion from wood is perfect by the end of the simulation. In the parallel reactions model, char is mainly produced by lignin pyrolysis, and according to the employed kinetic model [32], this process continues to higher temperatures than what can be achieved in cone calorimeter. Therefore, while using the parallel reactions model, the conversion from lignin to char is imperfect at the end of simulation.

The emissivity ε of virgin wood is assumed as 0.9 [41], the convective heat transfer coefficient in the cone calorimeter is assumed as 15 W/(m^{2}K), being the average of the literature range of 10 W/(m^{2}K) to 20 W/(m^{2}K) reported by Ryder and Weckman [42], the specific heat of char is assumed to follow the correlation presented by Fredlund [43] (Equation 5), and the specific heat of wood to follow the experimental results of Rinta-Paavola and Hostikka [32] (Equation 6). In this research, we assume thermal conductivity of char according to a correlation by Alves and Figueiredo [44], presented as Equation 7. The correlation is based on their experiments on *Pinus pinaster* char, which we assume as similar to Norway spruce and Scots pine.

$$c_{p,char} = 1430 + 0.355T - \frac{7.32 \cdot 10^7}{T^2}\ (\mathrm{J/kgK}) \tag{5}$$

$$c_{p,wood} = 4.4T - 414\ (\mathrm{J/kgK}) \tag{6}$$

$$k_{char} = 8.2 \cdot 10^{-5}T + 0.091\ (\mathrm{W/mK}) \tag{7}$$

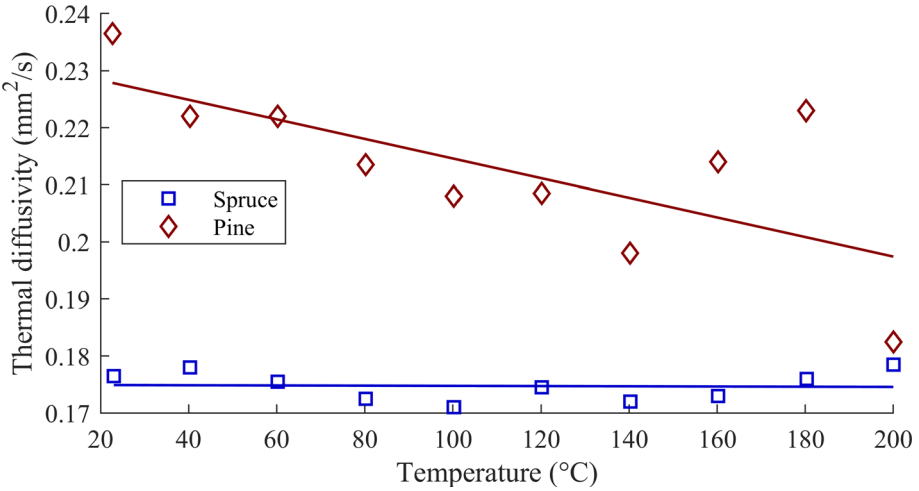

Figure 3. Thermal diffusivity of spruce and pine measured using laser flash analysis.

where T is the absolute temperature.

Figure 3 presents the average experimental thermal diffusivity as a function of temperature for spruce and pine measured with laser flash analysis, and their respective linear fits. Using the wood specific heat capacity according to Equation 6, thermal conductivity of spruce and pine are calculated from the linear fits to thermal diffusivity, and presented as Equations 8 and 9, respectively.

$$k_{spruce} = 3.16 \cdot 10^{-4} T - 0.0305\,(\mathrm{W/mK}) \tag{8}$$

$$k_{pine} = 3.57 \cdot 10^{-4} T - 0.00462\,(\mathrm{W/mK}) \tag{9}$$

where T is the absolute temperature.

The char reaction order with respect to oxygen is assumed as 0.68 [45] and the gas diffusion length scale L_g in Eqyation 3 is set at 10^{-4} m to restrict oxygen penetration within the charring wood near the exposed surface. The chosen diffusion length scale is close to the length of a single solid phase grid cell in the simulations employed in this work, which effectively turns the volumetric oxidation to a surface reaction. In the absence of a detailed mass transfer model for oxygen diffusion, this is a common method of modelling char oxidation, e.g. [24, 46]. Further, the detailed simulation results in the supplementary material of Richter and Rein [26] reveal that, in conditions similar to our simulations, oxygen is very efficiently consumed at a thin reaction front, and it cannot penetrate into any deeper into the char layer.

Regarding the energetics, we assume a heat of oxidation of − 32,000 kJ/kg for char [47]. Heats of combustion in gaseous phase ΔH_c are assumed the same as

determined in [32] and presented in Table 2. The table shows for completeness the kinetic parameters for wood pyrolysis estimated in earlier work [32], which are employed also herein. In [32], the kinetic parameters were estimated using thermogravimetric experiments, which are readily available in the referred work. Of the symbols not declared earlier in the paper, v_{char} is the char yield.

At the exposed boundary in the cone calorimeter model, the incident heat flux is defined in each case as the nominal radiative heat flux from the cone. While simulating the experiments in oxygen-free nitrogen atmosphere and in smoldering conditions, computational fluid dynamics modelling of the gaseous phase was turned off to save a significant amount of computational time, as it was found to have negligible impact on simulation results. In these conditions, the surrounding oxygen content was assumed either as zero or the standard atmospheric value, respectively, the gas temperature being assumed as the ambient temperature of 27°C in both. The computational fluid dynamics calculation of the gaseous phase was turned on during simulations of the experiments in flaming conditions to allow modelling of the flame, and it was allowed to freely predict local time dependent gas phase temperatures and oxygen concentrations, the initial state being standard atmosphere at the ambient temperature of 27°C. As the unexposed side boundary condition, we have modelled the ceramic wool layer of 1.3 cm the specimen rests upon. The back side of the wool is facing the ambient temperature of 27°C and is defined the same convective heat transfer coefficient of 15 W/(m^{2}K) as the exposed surface. Defining a physically accurate boundary condition for the back side of the wool would be difficult, but we deem the current choice justified, as in the experimental conditions the wool is placed in a highly conductive steel sample holder, and in oxygen-free conditions all of the nitrogen flow is coming from below the specimen level, and so is great part of ambient replacement air during operation in standard atmosphere.

3.2. Pyrolysis Rate in Nitrogen Atmosphere

Figures 4 and 5 present experimental mass loss and measured temperatures, respectively, for both woods in cone calorimeter experiments in nitrogen atmosphere under heat flux of 35 kW/m^2, and the predictions of single-, and parallel reactions models fitted to these experiments. The single reaction model for spruce, excluding its oxidative component, is estimated using solely these experiments, while the rest of the alternative models were estimated using simultaneously experiments in smoldering and flaming conditions, which are presented later. As model validation, Figure 6 presents the experimental mass loss rate in the same atmosphere under heat flux of 50 kW/m^2, and the corresponding predictions by models fitted to experiments in 35 kW/m^2. Table 3 shows the relative root mean square error (RRMSE) for model predictions of mass loss rate and specimen temperature. Throughout this work, the initial temperature of 27°C is assumed as the zero level for calculating RRMSE for temperature predictions.

Under the heat flux level of 35 kW/m^2, Table 3 shows a better fit for parallel reactions model for spruce. Conversely, with pine, the single reaction model offers significantly better fit. However, based on assessment of Figure 4, we conclude

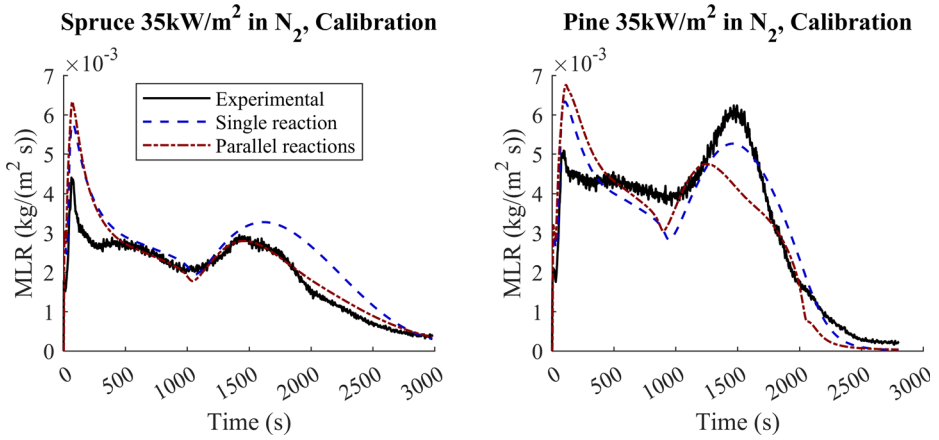

Figure 4. Experimental mass loss rates (MLR) in cone calorimeter under 35 kW/m^2 and nitrogen atmosphere, and corresponding predictions by estimated models.

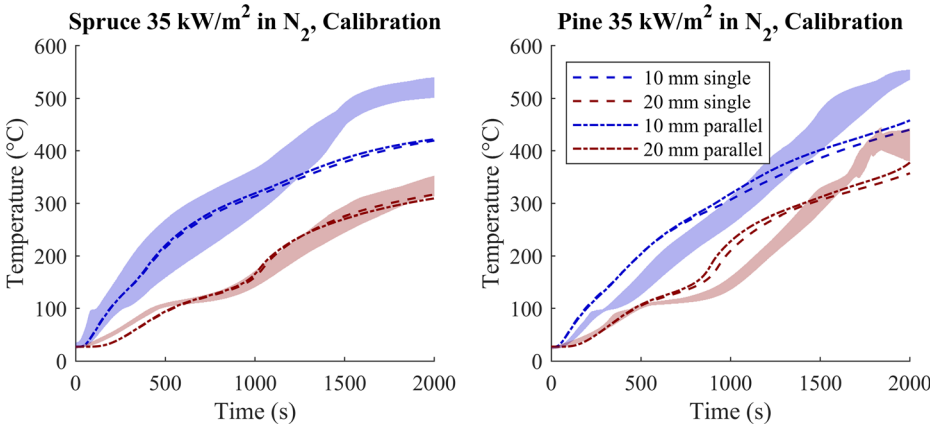

Figure 5. Experimental temperatures in cone calorimeter under 35 kW/m^2 and nitrogen atmosphere, and corresponding predictions by estimated models. Variation in experimental results in shaded area.

both the single-, and parallel reactions models of both spruce and pine to provide an acceptable fit, as the locations of mass loss rate peaks are accurately predicted and the predicted mass loss rates lie in the correct magnitude. The main exception is the first mass loss peak, which is systematically above the experimental level in all simulations in nitrogen atmosphere. The most likely cause is the models assuming instantaneous mass transfer for released volatiles, whereas in reality, evaporating moisture and wood decomposition products released early in the experiment will experience mass transfer limitations, thus increasing their residence time inside

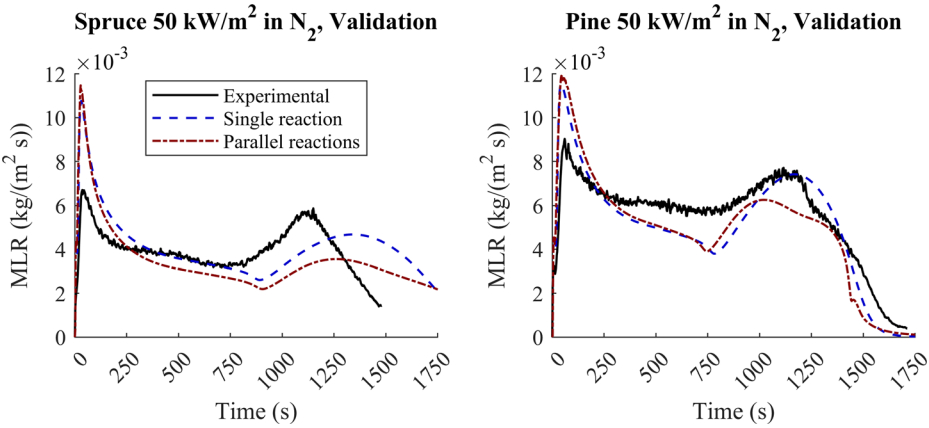

Figure 6. Experimental mass loss rates in cone calorimeter under 50 kW/m^2 and nitrogen atmosphere, and corresponding model validations.

Table 3
Relative Root Mean Square Errors for Model Predictions of Mass Loss Rate (MLR) and Specimen Temperature (T) in Simulations of Experiments Under Nitrogen Atmosphere

	Spruce		Pine	
Experiment	Single reaction (%)	Parallel reactions (%)	Single reaction (%)	Parallel reactions (%)
MLR, 35 kW/m^2	35	28	18	43
T, 10 mm, 35 kW/m^2	19	19	19	16
T, 20 mm, 35 kW/m^2	7	7	16	15
MLR, 50 kW/m^2	35	36	20	24

the specimen. Table 3 shows a higher RRMSE for temperature measurements at 10 mm depth than at 20 mm throughout, but especially for both model predictions of spruce. This could be mainly assigned for underpredicted temperature compared to the experiment near the end of simulation, which is most likely caused by crack formation in the char layer in the later stage of the real experiment. Cracks strongly enhance heat transfer deeper into the wood, but their formation is not included in the current models. When observing the mass loss rates under 50 kW/m^2, the most notable exception is that Figure 6 shows slightly delayed second mass loss rate peaks for predictions of both single-, and parallel reactions models for spruce. This translates to slightly increased RRMSE for the

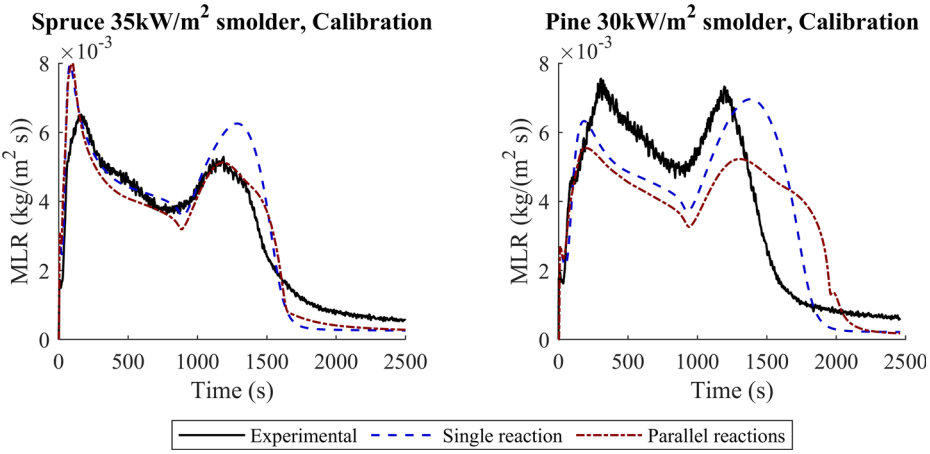

Figure 7. Experimental mass loss rates in cone calorimeter under 35 (spruce) or 30 (pine) kW/m² in smoldering conditions, and corresponding predictions by estimated models.

parallel reactions model compared to prediction at 35 kW/m^2, but for the single reaction model, the value remains unchanged. Despite this, we consider the quality of the fit acceptable when considering the other parts of the model as well.

3.3. Smoldering Combustion

Figure 7 presents experimental mass loss rates in smoldering conditions in standard atmosphere used for model estimation, under heat flux levels of 35 and 30, for spruce and pine, respectively, and the corresponding fitted models. As model validation, Figure 8 presents experimental and predicted mass loss rates in smoldering conditions under heat flux level of 25 or 20 kW/m^2, for spruce and pine. Table 4 presents relative root mean square errors for model predictions of mass loss rates in these conditions. Only spruce is tested at a same heat flux level (35 kW/m^2) in both oxygen-free and smoldering conditions. Comparison of spruce results in Figures 4 and 7 present the effect of surface oxidation most clearly, the mass loss rate being higher and the peaks occurring earlier in the presence of oxygen, which is also captured by the models. Table 4 shows the pine validation simulations under 20 kW/m^2 as the main discrepancy, both with the single-, and parallel reactions models. Figure 8 shows the predicted mass loss rates of pine to be significantly below the experimental level for most of the simulation. A likely reason is the heat flux level being already rather low, and the model estimated to experiments at higher heat fluxes might not transfer perfectly to these conditions.

3.4. Flaming Combustion

Enabling the gaseous phase and thus flaming combustion in simulations during the model estimation is computationally prohibitively expensive. To reduce the computational cost over the course of the estimation process, we employed the

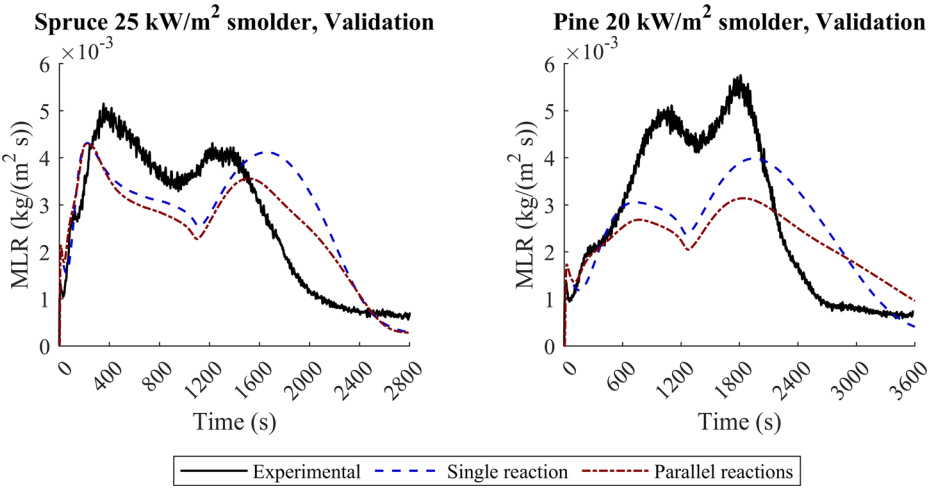

Figure 8. Experimental mass loss rates in cone calorimeter under 25 (spruce) or 20 (pine) kW/m² in smoldering conditions, and corresponding model validations.

Table 4
Relative Root Mean Square Errors for Model Predictions of Mass Loss Rate (MLR) in Simulations of Experiments in Smoldering Conditions

	Spruce		Pine	
Experiment	Single reaction (%)	Parallel reactions (%)	Single reaction (%)	Parallel reactions (%)
MLR, 25/20 kW/m²	41	35	45	51
MLR, 35/30 kW/m²	26	20	42	43

method presented by Korhonen et al. [48]. (The original source is in Finnish, but a brief presentation in English may be found at [49]). A number of FDS simulations of a burner with different specified heat release rates and surface temperatures, representative of different stages of the cone calorimeter experiment, were carried out first, and the corresponding flame heat fluxes were obtained from the simulation output. Table 5 presents the estimated flame heat fluxes at different times of flaming cone calorimeter experiments of spruce and pine at 35 kW/m². These flame heat fluxes were implemented into the FDS models as RAMP-function -controlled external heat fluxes, assuming a linear change between data points.

Table 5
Flame Heat Flux at Cone Calorimeter Experiments of Spruce and Pine in Flaming Conditions Under Heat Flux Level of 35 kW/m^2, Estimated According to [48]

Spruce		Pine	
Time (s)	Heat flux (kW/m^2)	Time (s)	Heat flux (kW/m^2)
0	0	0	0
14	0	30	0
40	20.8	48	21
60	21.2	80	21.5
80	21.8	177	21.9
200	24.3	250	23.9
350	22.3	780	24.2
700	22.3	900	21
844	24.4	1010	21.3
1050	21.3	1100	20.9
1200	23.1	1250	20
1290	18.3		

However, this method does not take into account the attenuation of external heat flow through the flame. In their research, Li et al. [50] embedded a heat flux gauge at the center of a medium density fibreboard (MDF) specimen tested under a cone calorimeter in flaming conditions. In their test on a MDF specimen under 35 kW/m^2 with a setup that is most comparable to this research (experiment 11 in [50]), the additional measured heat flux from flaming was in the order of 20 kW/m^2 during the heat release peaks, and a bit under 10 kW/m^2 during steady burning. We assume this may be generalized to the currently tested woods as well, the MDF in [50] consisting of 90% radiata pine. A comparison between Table 5 and the steady burning flame heat flux in [50] suggests considerable blocking of external radiation by flames. Nevertheless, used the computed flame heat fluxes as such because we deem this method to be more consistent with the final flaming cone calorimeter simulations where the attenuation of external radiation is neither considered, the incident heat flux equal to nominal cone heat flow being set as a boundary condition. Further, FDS Validation Guide [51] reports the model relative standard deviation for wall, ceiling and floor heat flux predictions as 27%. Properly addressing the issue of blocking of the external heat flux by flames would require detailed solution of the flame radiative characteristics, which is outside the scope of this study.

The final simulation results in flaming conditions presented in Figures 9, 10, 11, 12, 13, 14 and 15 were obtained with gaseous phase model turned on, thus including flaming combustion. As the raw heat release rate output in FDS only considers the gas phase combustion, they were supplemented with heat released by char oxidation, obtained by multiplying char mass loss rate with its heat of oxidation. This allows for the comparison of measured and simulated heat release rates after

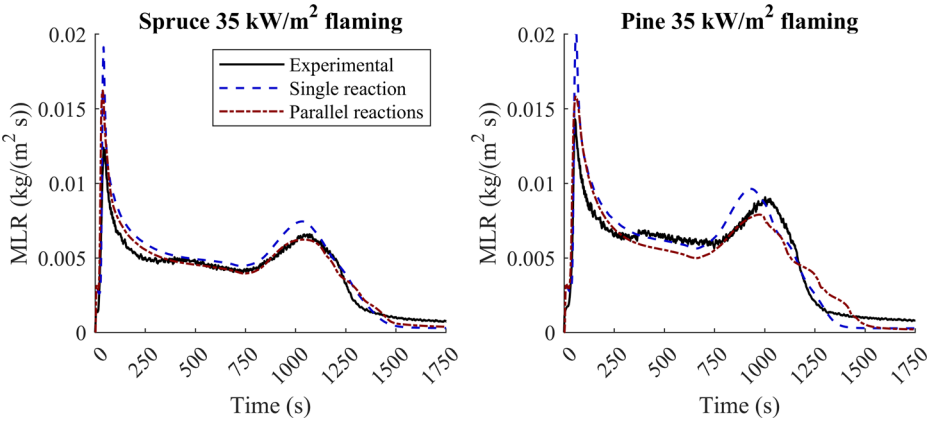

Figure 9. Experimental mass loss rates in cone calorimeter under 35 kW/m² and flaming conditions, and corresponding predictions by estimated models.

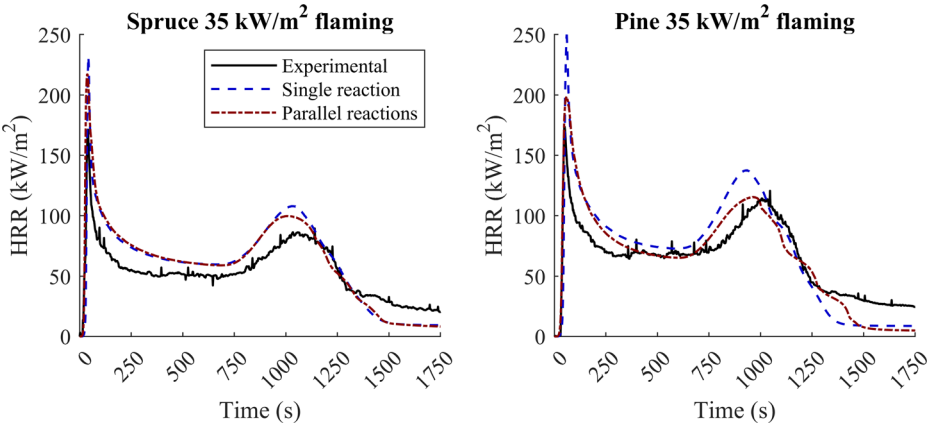

Figure 10. Experimental heat release rates (HRR) in cone calorimeter under 35 kW/m² and flaming conditions, and corresponding predictions by estimated models.

transition from flaming combustion to smoldering. As per the operation principle of the cone calorimeter, it considers all released carbon dioxide to participate in experimental heat release rate, including that originating from oxidation of char.

Figures 9, 10 and 11 presents measured and simulated mass loss rates, heat releases rate and temperatures inside and on the unexposed side of the specimen, respectively, in cone calorimeter experiments in flaming conditions and under heat flux level of 35 kW/m^2. For the single reaction model of spruce, experiments in flaming conditions serve purely as validation, as the model is estimated using experiments in nitrogen and in smoldering conditions, with heats of combustion

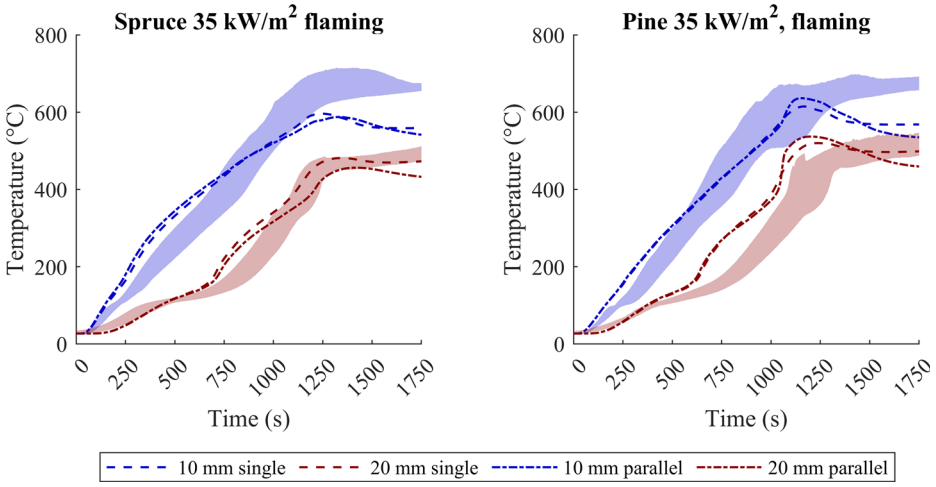

Figure 11. Experimental temperatures in cone calorimeter under 35 kW/m² and flaming conditions, and corresponding predictions by estimated models. Variation in experimental results in shaded area.

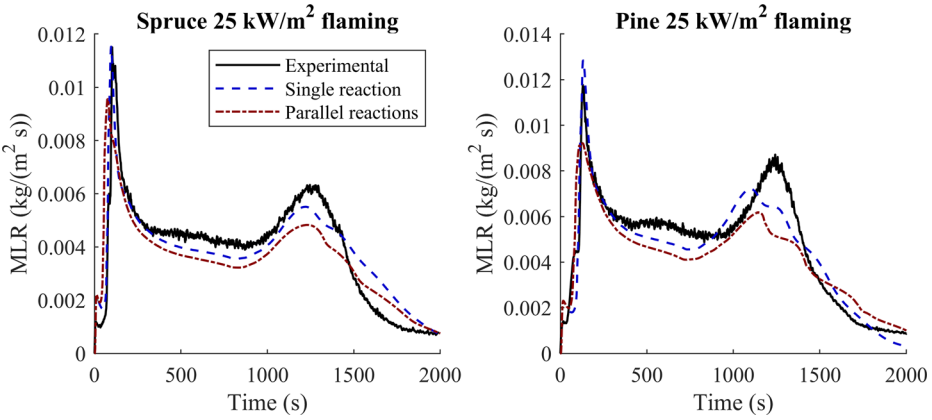

Figure 12. Experimental mass loss rates in cone calorimeter under 25 kW/m² and flaming conditions, and corresponding predictions by estimated models.

presented in Table 2. For the rest of the models, experimental mass loss rate and specimen temperatures under 35 kW/m^2 are used in model estimation.

For model validation purposes, Figures 12 and 13 present mass loss and heat release rates, for the flaming experiments and simulations under 25 kW/m^2, and Figures 14 and 15 correspondingly for 50 kW/m^2. Table 6 shows the relative root mean square errors of predictions of mass loss rates, heat release rates and specimen temperatures in flaming conditions. Figures 9, 10, 11, 12, 13, 14 and 15 and Table 6 prove accurate model fit throughout in flaming conditions. Regarding

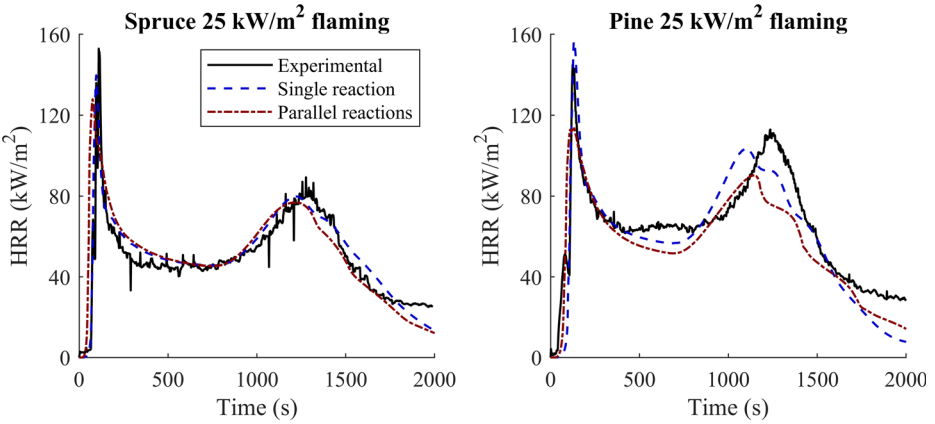

Figure 13. Experimental heat release rates in cone calorimeter under 25 kW/m² and flaming conditions, and corresponding predictions by estimated models.

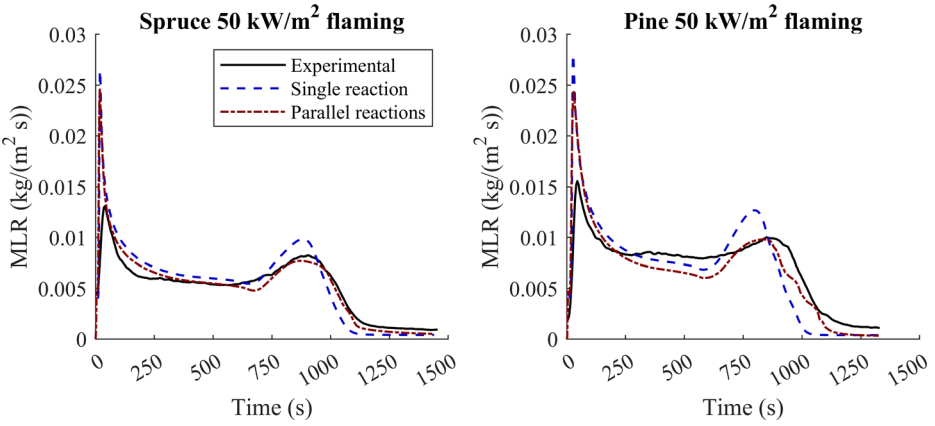

Figure 14. Experimental mass loss rates in cone calorimeter under 50 kW/m² and flaming conditions, and corresponding predictions by estimated models.

specimen temperatures in spruce under 35 kW/m^2, we make a similar observation as in non-oxidative conditions under nitrogen atmosphere: RRMSE is higher for the simulated temperature at 10 mm depth than at 20 mm, caused by the underpredicted temperature near the end of the simulation. Temperature at 10 mm inside the pine specimen shares a similar behavior, even though there the temperature predictions at 20 mm exhibit a higher RRMSE caused by overprediction of the temperature for most of the simulation. This consistent behavior of temperature at 10 mm depth inside the specimen supports our conclusion about the crack formation not included in the model being the root cause for the disagreement.

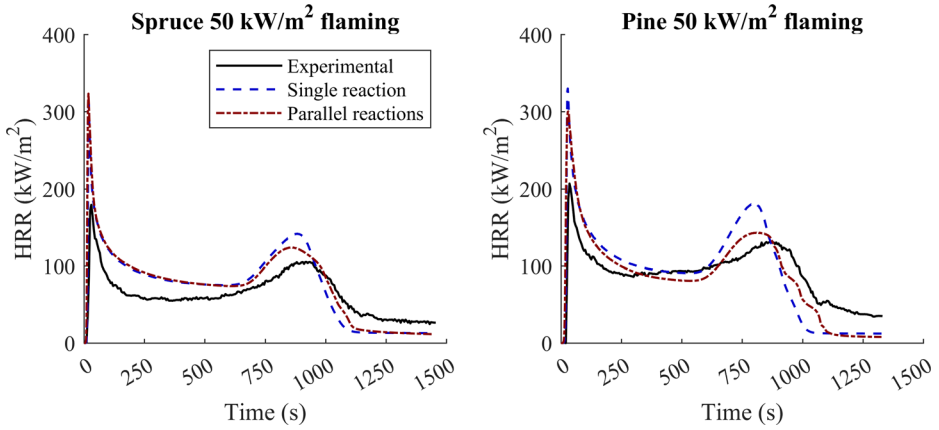

Figure 15. Experimental heat release rates in cone calorimeter under 50 kW/m^2 and flaming conditions, and corresponding predictions by estimated models.

Table 6
Relative Root Mean Square Errors for Model Predictions of Mass Loss Rate (MLR), Heat Release Rate (HRR) and Specimen Temperature (T) in Simulations of Experiments in Flaming Conditions

	Spruce		Pine	
Experiment	Single reaction (%)	Parallel reactions (%)	Single reaction (%)	Parallel reactions (%)
MLR, 25 kW/m^2	20	29	17	25
HRR, 25 kW/m^2	16	28	20	22
MLR, 35 kW/m^2	23	19	22	21
HRR, 35 kW/m^2	32	33	35	27
T, 10 mm, 35 kW/m^2	18	20	15	16
T, 20 mm, 35 kW/m^2	16	13	28	32
MLR, 50 kW/m^2	35	30	37	28
HRR, 50 kW/m^2	47	47	40	32

3.5. Summary of Cone Calorimeter Experiments

The results in cone calorimeter scale reveals the near-equal quality of fit between the single-, and parallel reactions models for both species of wood across all

experimental conditions. Rinta-Paavola and Hostikka [32] concluded, that the parallel reactions model would not offer any advantage over the single-reaction model, but arriving with the added cost of model complexity, and hence uncertainty. However, in that research they used only measurement data that are integral in nature, namely heat release and mass loss, reserving investigating possibility of the parallel reactions model to predict local temperatures and char front progress better as a future research topic. The current results with the internal temperature measurements do not change their previous conclusion: the single reaction model is the preferable option, offering similar performance to the parallel reactions model without its increased model uncertainty.

3.6. Large Scale Validation

The models are tested by applying it in prediction of temperature evolution inside timber assemblies in macroscopic scale furnace fire tests [52, 53], as opposed to mesoscopic cone calorimeter tests. The modeled tests from the work of König and Walleij [52] (tests C1 to C3 as per their nomenclature, all replications with the same set-up) were performed on a 95 mm thick assembly of spruce planks, the hot boundary being a parametric fire, that in reality followed the ISO 834 fire until reaching a peak temperature at 30 min. The observed test by VTT Expert Services [53] is on temperature development inside a 195 mm thick solid timber assembly, the hot gas boundary condition following the ISO 834 fire curve. The wood species is not explicitly declared, but the announced wet density of 483 kg/m^3 with a moisture content of 8% by mass leads us to believe the tested specimen is spruce.

For the simulation of both of the tests [52, 53], the oxygen concentration inside the furnace was assumed as 7% by volume, based on Babrauskas [11] claiming a range of 4% to 10% for oxygen concentration in fire testing furnaces. We carried out the simulations using the smoldering model for spruce, which we justify by the fire testing furnace being a very turbulent environment, disrupting any flame from the wood specimen itself, and keeping the conditions on the specimen boundary and the ambient of the furnace close to each other. To model radiative and convective heat flux to the exposed timber, we specified the gas phase temperature and the surrounding radiation temperature to correspond to the gas phase temperature programs in the experiments. In both tests, convective heat transfer coefficient within the furnace is assumed as 25 W/(m^{2}K) in accordance with Eurocode 1, Part 1–2 [7]. On the unexposed side, we assume a gas temperature of 20°C, which is close to the ambient value in both. The same relatively high convective heat transfer coefficient of 25 W/(m^{2}K) is assigned also on the unexposed side. However, we estimate any error leading from this as negligible, because according to the simulations the temperature rise on the unexposed side is insignificant over the length of the experiments.

Figures 16 and 17 compare experiments of König and Walleij [52] and VTT Expert Services [53], respectively, to their corresponding simulations, using both the single and parallel reaction models for spruce. Unlike König and Walleij [52], VTT Expert Services [53] conducted a single test but installed two thermocouples for each depth. In the figures, shaded areas represent experimental variation

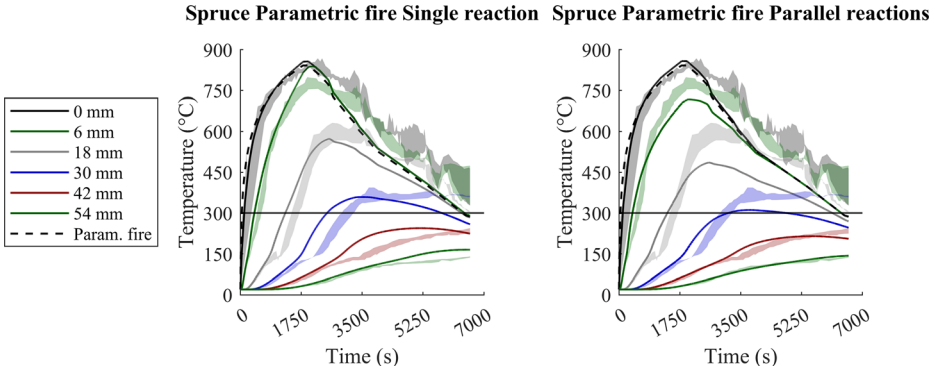

Figure 16. Temperatures inside timber at various depths during tests C1 to C3 [52], with shaded areas indicating experimental variability and corresponding model predictions in solid lines. The employed parametric fire in dashed line as a reference, with its first 30 min replaced by ISO 834 temperature curve. A black horizontal line represents the 300°C isotherm, which is assumed as the charring temperature.

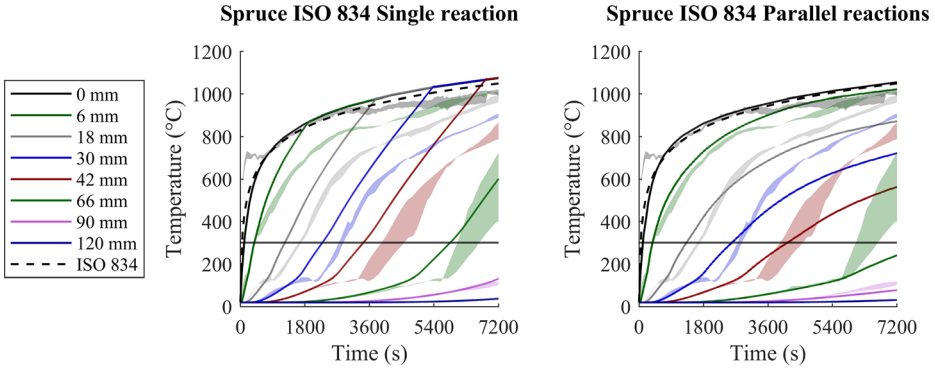

Figure 17. Temperatures inside timber at various depths during ISO 834 test [53], with shaded area indicating variability between thermocouples at each depth, and corresponding model predictions in solid lines. ISO 834 temperature curve in dashed line for reference. A black horizontal line represents the 300°C isotherm.

between different tests or different thermocouples at the same depth. The figure legends declare the distance of the thermocouple from the exposed surface. For comparison, Figure 18 presents the model predictions for pine wood in ISO 834 conditions in a similar setup as in VTT Expert Services [53] experiment.

Figure 16 shows that the overall quality of fit to the experimental data by König and Walleij [52] is good and near-equal between both single-, and parallel reactions models. The main exception is, that the simulated final temperatures are closer to each other than in experiments. In the cooldown phase, many of their

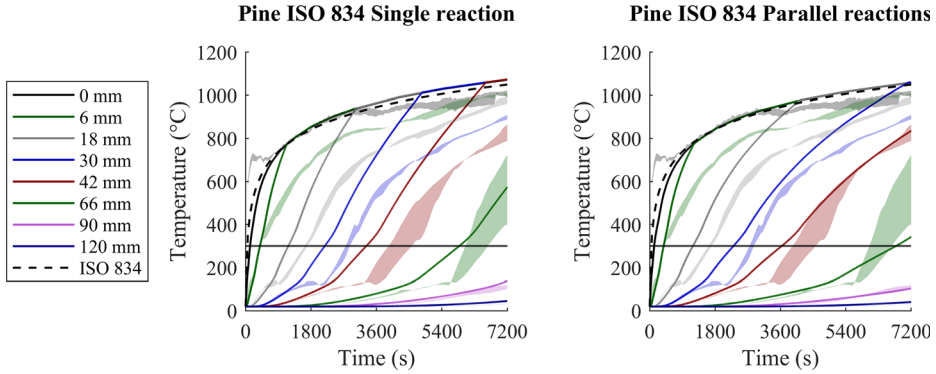

Figure 18. Simulation results with pine wood in a similar setup as in Figure 17 compared to the experimental results [53], that we assume are for spruce. A black horizontal line represents the 300°C isotherm.

thermocouples near the surface at multiple instances exhibit a temperature higher than the actual gas phase temperature at the same moment, which instead happens in neither of our model predictions to any significant effect. A possible cause for the discrepancy could be oxidation of char near the specimen surface. In the model, oxygen does not penetrate deep into the char. In reality, cracks may offer it an easy passage deep into the char, exothermic char oxidation maintaining higher temperatures in the solid near the surface than in the gaseous phase. Another likely reason for the discrepancy in temperatures would be differences in char contraction rates by oxidation in the experiments and simulations. In comparison, Richter et al. [27] have as well successfully employed their material model in predicting the experiment C3 of König and Walleij [52]. Richter et al. [27] have utilized a three-component model in their work (hemicellulose, cellulose, and lignin), each of them producing char, which in turn oxidizes. As a difference, however, they have enabled oxidation reactions for cellulose and hemicellulose as well. Also, their model is built in Gpyro [54] instead of FDS, which means it solves the species transport and conservation in porous media for oxygen and other gaseous phase species.

However, a significant disagreement appears when comparing ISO 834 fire test results [53] to the corresponding model predictions, as Figure 17 shows. Whereas the slopes of experimental temperature curves at each depth start to decrease after reaching 600°C, in the prediction by the single reaction model the curves maintain an almost linear growth until reaching the gas phase temperature, thus indicating char oxidation front reaching each measurement depth very much prematurely. With the parallel reactions model, the temperature increase remains notably below the experimental values, especially deeper inside the timber. Another observation is that the model results do not exhibit as significant temperature plateau at 100°C caused by water as in experiments. The suggested reason for this difference is the lack of a mass transfer model, the models instead assuming instantaneous trans-

Table 7
Relative Root Mean Square Errors for Predicted Times of Char Front Reaching Temperature Measurement Depths in the Parametric Fire [52] and ISO 834 [53] Tests, for Single-, and Parallel Reactions Models of Spruce

Experiment	Spruce, single reaction (%)	Spruce, parallel reactions (%)
Parametric fire [52]	25	11
ISO 834 [53]	19	30

port of any volatiles to the specimen surface. In the experiments, there may be a flow of moisture from the deeper wood, maintaining a constant temperature for an extended period of time.

Because already the visual observation of Figures 17 and 18 reveal that the estimated models could not be generalized to give prediction of temperature profile development in large scale, we deem more meaningful to specify model errors with respect to the charring rate instead, which is better predicted. Table 7 presents the RMSE for the predicted times for the char front (300°C) to reach different measuring depths in parametric fire (Figure 16) and ISO 834 (Figure 17) tests, for single -, and parallel reactions models for spruce. The observed depths are up to where the temperature passes 300°C during the experiment, that is 30 and 66 mm for the parametric fire and ISO 834 tests, respectively.

It is difficult to conclude, whether the single-, or parallel reactions model would be an optimal choice in predicting temperature profile in large timber assemblies under fire. Simulations of the experiments of König and Walleij [52] show little difference in temperature profile evolution between the single-, and parallel reactions models. On the other hand, the question of preferable model becomes highly ambiguous when comparing the simulations to the ISO 834 fire tests [53], as the predicted final temperatures are significantly off the experimental values with both models, but in opposite directions. Applying the pine single-, and parallel reactions models for the ISO 834 test, the simulation results turned out to differ significantly from the experiment, and we conclude that none of the models for pine are neither able to predict satisfactorily the internal temperature development in large scale.

In light of the above, we conclude that the proposed material models require further development before being applied in large scale. The main topics for future research for improving the model performance in prediction of temperatures inside burning timber, would be specifying mass transfer of evaporating moisture and pyrolysis products, and the properties of cracking char layer. These may not be very significant when modelling a 2 cm thick specimen in cone calorimeter, but for example, in the ISO 834 fire test in [53], the specimen is thicker approximately by a factor of ten. Therefore, the current assumption of instantaneous mass transfer to the specimen surface is likely to not hold any

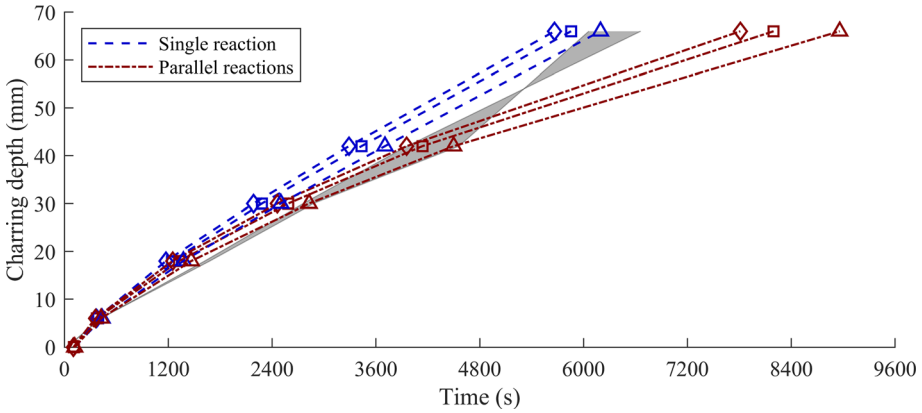

Figure 19. Sensitivity analysis of moisture concentration on char front progress. Experimental variation in shaded area [53], and simulations of spruce with moisture contents of 5, 8 (reference) and 15 wt% with diamond-, square-, and triangle-shaped markers, respectively.

more, and cracking of char layer starts to have more profound effect, cracks offering an easy passage for heat and oxygen.

We point out that even in its current state, the models for spruce are able to capture the progress of the 300°C isotherm inside a large scale specimen, however minding that the char front progress starts significantly delaying at greater depths with the parallel reactions model, as the simulated temperature at 66 mm depth in Figure 17 shows. Table 7 shows neither the single-, or parallel reactions models appearing superior to one another in prediction of char front progress, the single reaction model producing a poorer fit than the parallel reactions model to the parametric fire test, but a better to the ISO 834 test.

We test the sensitivity of single-, and parallel reactions models of spruce with respect to wood moisture content and furnace oxygen concentration in the ISO 834 test [53], and observe the effect on char front progress. We assume char front as the 300°C isotherm, following it up to the depth of 66 mm, as it is the final measurement point to reach 300°C before the end of the experiment. Figures 19 and 20 present sensitivity of char front progress to moisture content of wood and the oxygen concentration, respectively. The variation in wood moisture content is from 5 wt% to 15 wt%, and in furnace oxygen concentration from 4% to 10%, this being the span reported by Babrauskas [11]. The reference simulation in both figures is the same as in Figure 17, with a wood moisture content of 8% and the furnace oxygen concentration of 7%.

As expected, higher moisture content of the wood corresponds to a slower charring rate, but more drastic effects are present when varying the oxygen content of the furnace. Figure 20 shows that a variation of 3 percentage points in either direction within the expected furnace oxygen concentration range of 4 to 10%, leads to a difference of approximately 10 min in char front reaching the depth of

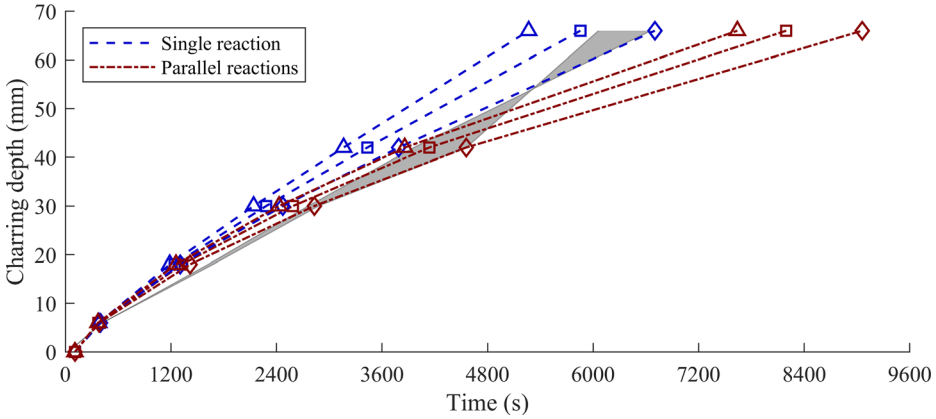

Figure 20. Sensitivity analysis of furnace oxygen concentration on char front progress. Experimental variation in shaded area [53], and simulations of spruce with oxygen concentrations of 4, 7 (reference) and 10% with diamond-, square-, and triangle-shaped markers, respectively.

66 mm, consistently for both single-, and parallel reactions models. Even though the models are not able to predict the final temperatures in ISO 834 -experiment accurately, this suggests the charring rate being significantly sensitive to the oxygen concentration in the furnace—a parameter that is rarely published in test reports of large scale fire experiments.

3.7. Wood Shrinkage on Cellular Level

Figure 21 presents the scanning electron microscope images from the same position in the spruce specimen before heat treatment (reference) and after pyrolysis in 250, 325, 400, 475 and 550°C. The shrinkage in early-, and latewood (left and right in the SEM images, respectively) in radial direction of the trunk, was evaluated by selecting a group of cells in both and measuring their length at each image. The groups of selected cells are indicated in each image by a white line. In earlywood, the group consists of 9 and in the latewood of 14 cells. In the reference image their lengths are 226 and 244 μm, respectively. Table 8 presents the observed shrinkage from the initial state after pyrolysis in each temperature.

Table 8 shows that, at lower temperatures, the latewood with thicker cell walls shrinks faster. Observing the SEM images of Figure 21 reveals that the early shrinkage is caused by thinning of the cell walls. However, after pyrolysis at the highest employed temperature of 550°C, the level of shrinkage in early-, and latewoods is near-equal.

The observed cellular level shrinkage is in conflict with the 12% average swelling of spruce specimens in oxygen-free cone calorimeter tests. To investigate the reason behind the different behaviors, we took charred specimens of spruce and pine, tested under nitrogen in cone calorimeter, and cut them open as shown in

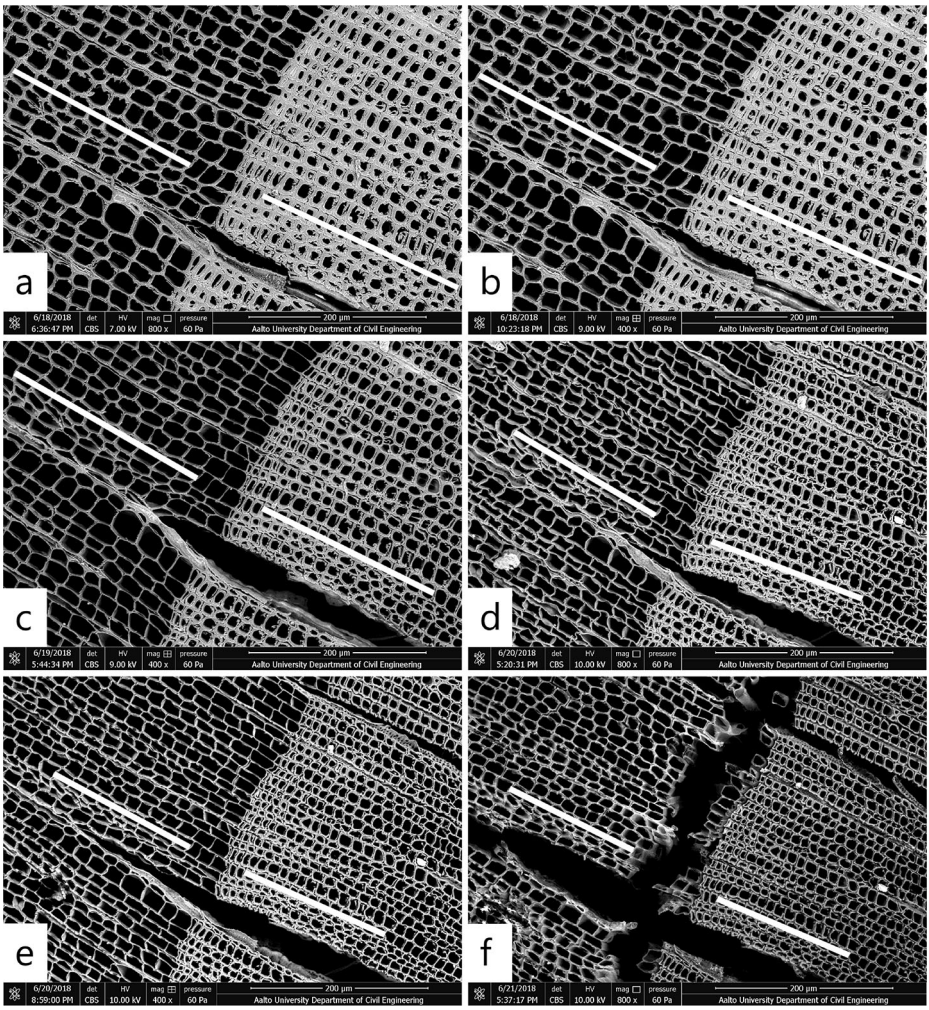

Figure 21. Scanning electron microscope images taken on the same location on a spruce wood specimen after pyrolysis in different temperatures. The images are (a) reference without thermal treatment, after pyrolysis at (b) 250°C, (c) 325°C, (d) 400°C, (e) 475°C and (f) 550°C. The scale bar is 200 µm in all images.

Figure 22. Spruce char appears highly porous because of numerous small cracks, whereas pine char appears more dense and continuous. The SEM image of spruce wood pyrolyzed at 550°C in Figure 22 may present one such crack. Therefore, we suggest the swelling of spruce timber in macroscopic scale being caused by the increasing void fraction inside the specimen, even though its cellular structure is shrinking.

Table 8
Spruce Early-, and Latewood Shrinkage in Radial Trunk Direction After Pyrolysis at Different Temperatures, Observed from Scanning Electron Microscope Images

Pyrolysis temperature (°C)	Shrinkage, earlywood (%)	Shrinkage, latewood (%)
Reference	0	0
250	0	0
325	6	11
400	18	27
475	23	29
550	32	34

Figure 22. Charred specimens of spruce (left) and pine (right) after cone calorimeter testing in nitrogen, opened. The grain direction is towards the reader. The image brightness is adjusted in the specimen region to better reveal the char structure.

4. Conclusions

Material models describing pyrolysis, oxidation and flaming combustion of Norway spruce and Scots pine, two widely used structural timbers, have been developed. A set of two separate models were estimated for both species of wood; one that assumes the wood as a single homogenous component (single reaction), and another that assumes the wood as a mixture of its principal chemical components of hemicellulose, cellulose and lignin, each one of them decomposing independently to form char (parallel reactions). The exothermic oxidation reaction of wood char was included in the model.

The model parameters were estimated using experimental results in cone calorimeter tests, subjecting the wood to different conditions: pyrolysis in near oxygen-free nitrogen atmosphere, smoldering conditions in standard atmosphere, and in flaming conditions.

We did not observe significant differences in performance between the single-, and parallel reactions models in the cone calorimeter scale. The work of Rinta-Paavola and Hostikka [32] arrived at the conclusion of the single reaction model being preferable option, for minimizing the model uncertainty while having near-

equal performance to the parallel reactions model. The current work supports this conclusion, as not even the more detailed experiments presented in this paper can support the more complex parallel reactions model, at least in the cone calorimeter scale. The parallel reactions model however may find use in calculating the remaining strength of wood under fire, as Adibaskoro et al. [35] found the decline in the wood mechanical strength and its shrinkage by pyrolysis to coincide with hemicellulose and cellulose pyrolysis, respectively.

The developed models for spruce can reasonably predict the charring depth in ISO 834 test [53], but are not able to capture the details of the temperature histories, such as the water evaporation plateaus, or high temperatures inside the char layer. Further required improvements would be incorporation of mass transfer and crack formation into the model, cracking of the char layer having a significant effect on the charring and burning rates. The effect of char cracking is also visible in the cone calorimeter experiments, where the simulated temperatures fall significantly behind the experimental at the 10 mm depth near the end of the experiment. Therefore, we suggest a detailed observation of crack formation on charring wood as a topic for future research. Even though the char cracking would not be directly implemented to a fire simulation software, such as FDS, the results could be used in determining the effects of cracking by other means, such as estimation of effective thermal properties for char. Also, an important aspect of the performance of the proposed models would be their ability to predict fire spread. Investigating it was however not within the scope of this paper, and it is suggested as a topic for the future research.

The predicted charring rates in the large scale are shown to be highly sensitive to the surrounding oxygen concentration, and a change of 3 percentage points leads to a difference of approximately 10 min for the char front to reach the 66 mm depth. Even though the proposed models are not able to capture the final temperatures in the VTT Expert Services experiment [53], in the authors' opinion this is a sufficient proof for importance of the surrounding oxygen concentration for the charring rate. Therefore, our recommendation is to declare the furnace oxygen content in the test report whenever if feasible, which as of now is not the current practice.

Our study has shown the spruce timber to swell when charring in absence of oxygen, which is contrary to the common expectation of wood to shrink as it chars. Our results show the apparent swelling in macroscopic scale is caused by small cracks that increase the void fraction inside the specimen. This behavior should be taken into account in future works when modelling spruce wood under fire.

Acknowledgements

The authors wish to thank Professor Ari Jokilaakso in arranging us the possibility to conduct the laser flash analysis experiments, D.Sc. Anna Antonova for assistance in taking scanning electron microscope images, and D.Sc. Esko Mikkola for providing us with the fire test data from VTT Expert Services. The work has been

funded by the Academy of Finland under grant 297030 and by the Fire Protection Fund, Finland under Grant VN/14174/2021. This study utilized the Academy of Finland's RawMatTERS Finland Infrastructure (RAMI) based at Aalto University, GTK Espoo, and VTT Espoo. The authors wish to acknowledge CSC – IT Center for Science, Finland, for computational resources.

Funding

Open Access funding provided by Aalto University.

Declarations

Conflict of interest The authors have no relevant financial or non-financial interests to disclose.

Open Access

References

1. Östman B, Brandon D, Frantzich H (2017) Fire safety engineering in timber buildings. Fire Saf J 91:11–20. https://doi.org/10.1016/j.firesaf.2017.05.002
2. Ronquillo G, Hopkin D, Spearpoint M (2021) Review of large-scale fire tests on cross-laminated timber. J Fire Sci 39(5):327–369. https://doi.org/10.1177/07349041211034460
3. Xu H, Pope I, Gupta V, Cadena J, Carrascal J, Lange D, McLaggan MS, Mendez J, Osorio A, Solarte A, Soriguer D, Torero JL, Wiesner F, Zaben A, Hidalgo JP (2022) Large-scale compartment fires to develop a self-extinction gesign framework for mass timber—Part 1: Literature review and methodology. Fire Saf J 128:103523. https://doi.org/10.1016/j.firesaf.2022.103523
4. Mitchell H, Kotsovinos P, Richter F, Thomson D, Barber D, Rein G (2022) Review of fire experiments in mass timber compartments: current understanding, limitations, and research gaps. Fire Mater . https://doi.org/10.1002/fam.3121

5. Bal N, Rein G (2013) Relevant model complexity for non-charring polymer pyrolysis. Fire Saf J 61:36–44. https://doi.org/10.1016/j.firesaf.2013.08.015
6. European Committee for Standardization (2004) EN 1995-1-2:2004 Eurocode 5: design of timber structures—Part 1–2: General—Structural fire design. European Committee for Standardization, Brussels
7. European Committee for Standardization (2002) EN 1991-1-2:2002 Eurocode 1: actions on structures—Part 1–2: General actions—Actions on structures exposed to fire. European Committee for Standardization, Brussels
8. Hakkarainen T (2002) Post-flashover fires in light and heavy timber construction compartments. J Fire Sci 20(2):133–175. https://doi.org/10.1177/0734904102020002074
9. Salminen M (2015) Numerical analysis of charring of timber structures in natural fires. In: Kiviluoma R et al. (eds) IABSE workshop: safety, robustness and condition assessment of structures. International Association for Bridge and Structural Engineering, Zürich, pp 104–111. https://doi.org/10.2749/222137815815622735
10. Mikkola E (1991) Charring of wood based materials. In: Cox G, Langford B (eds) Fire safety science: Proceedings of the third international symposium. International Association for Fire Safety Science, London, pp 547–556. https://doi.org/10.3801/IAFSS.FSS.3-547
11. Babrauskas V (2005) Charring rate of wood as a tool for fire investigations. Fire Saf J 40(6):528–554. https://doi.org/10.1016/j.firesaf.2005.05.006
12. Lau PWC, White R, Van Zeeland I (1999) Modelling the charring behaviour of structural lumber. Fire Mater 23(5):209–216. https://doi.org/10.1002/(SICI)1099-1018(199909/10)23:5<209::AID-FAM685>3.0.CO;2-A
13. Franssen J-M (2005) SAFIR: a thermal/structural program for modeling structures under fire. Eng J 42(3):143–150
14. Cachim PB, Franssen J-M (2010) Assessment of Eurocode 5 charring rate calculation methods. Fire Technol 46(1):169–181. https://doi.org/10.1007/s10694-009-0092-x
15. Hopkin DJ, El-Rimawi J, Silberschmidt V, Lennon T (2011) An effective thermal property framework for softwood in parametric design fires: comparison of the Eurocode 5 parametric charring approach and advanced calculation models. Constr Build Mater 25(5):2584–2595. https://doi.org/10.1016/j.conbuildmat.2010.12.002
16. Pečenko R, Svensson S, Hozjan T (2015) Modelling heat and moisture transfer in timber exposed to fire. Int J Heat Mass Transf 87:598–605. https://doi.org/10.1016/j.ijheatmasstransfer.2015.04.024
17. Pečenko R, Svensson S, Hozjan T (2016) Model evaluation of heat and mass transfer in wood exposed to fire. Wood Sci Technol 50:727–737. https://doi.org/10.1007/s00226-016-0813-5
18. Pečenko R, Planinc I, Svensson S, Hozjan T (2019) Implementing coupled heat and moisture transfer model in the fire analysis of timber beams. Fire Saf J 107:170–178. https://doi.org/10.1016/j.firesaf.2018.11.007
19. Pečenko R, Hozjan T (2021) A novel approach to determine charring of wood in natural fire implemented in a coupled heat-mass-pyrolysis model. Holzforschung 75(2):148–158. https://doi.org/10.1515/hf-2020-0081
20. Kung H-C (1972) A mathematical model of wood pyrolysis. Combust Flame 18(2):185–195. https://doi.org/10.1016/S0010-2180(72)80134-2
21. Atreya A (1983) Pyrolysis, ignition and fire spread on horizontal surfaces of wood. Dissertation, Harvard University
22. Moghtaderi B, Novozhilov V, Fletcher D, Kent JH (1997) An integral model for the transient pyrolysis of solid materials. Fire Mater 21:7–16. https://doi.org/10.1002/(SICI)1099-1018(199701)21:1<7::AID-FAM588>3.0.CO;2-T

23. Spearpoint MJ, Quintiere JG (2000) Predicting the burning of wood using an integral model. Combust Flame 123(3):308–325. https://doi.org/10.1016/S0010-2180(00)00162-0
24. Lautenberger C, Rein G, Fernandez-Pello C (2006) The application of a genetic algorithm to estimate material properties for fire modeling from bench-scale fire test data. Fire Saf J 41(3):204–214. https://doi.org/10.1016/j.firesaf.2005.12.004
25. Lautenberger C, Fernandez-Pello C (2009) A model for the oxidative pyrolysis of wood. Combust Flame 156(8):1503–1513. https://doi.org/10.1016/j.combustflame.2009.04.001
26. Richter F, Rein G (2020) A multiscale model of wood pyrolysis in fire to study the roles of chemistry and heat transfer at the mesoscale. Combust Flame 216:316–325. https://doi.org/10.1016/j.combustflame.2020.02.029
27. Richter F, Kotsovinos P, Rackauskaite E, Rein G (2021) Thermal response of timber slabs exposed to travelling fires and traditional design fires. Fire Technol 57:393–414. https://doi.org/10.1007/s10694-020-01000-1
28. Li K, Mousavi M, Hostikka S (2017) Char cracking of medium density fibreboard due to thermal shock effect induced pyrolysis shrinkage. Fire Saf J 91:165–173. https://doi.org/10.1016/j.firesaf.2017.04.027
29. Li K, Hostikka S, Dai P, Li Y, Zhang H, Ji J (2017) Charring shrinkage and cracking of fir during pyrolysis in an inert atmosphere and at different ambient temperatures. Proc Combust Inst 36(2):3185–3194. https://doi.org/10.1016/j.proci.2016.07.001
30. Richter F, Jervis FX, Huang X, Rein G (2021) Effect of oxygen on the burning rate of wood. Combust Flame 234:111591. https://doi.org/10.1016/j.combustflame.2021.111591
31. McGrattan K, Hostikka S, Floyd J, McDermott R, Vanella M (2022) Fire dynamics simulator user's guide, revision: FDS6.7.9-0-gec52dee42. National Institute of Standards and Technology, Gaithersburg
32. Rinta-Paavola A, Hostikka S (2022) A model for the pyrolysis of two Nordic structural timbers. Fire Mater 46(1):55–68. https://doi.org/10.1002/fam.2947
33. Sjöström E (1981) Wood chemistry: fundamentals and applications. Academic Press, New York
34. Cape JA, Lehman GW (1963) Temperature and finite pulse-time effects in the flash method for measuring thermal diffusivity. J Appl Phys 34(7):1909–1913. https://doi.org/10.1063/1.1729711
35. Adibaskoro T, Makowska M, Rinta-Paavola A, Fortino S, Hostikka S (2021) Elastic modulus, thermal expansion, and pyrolysis shrinkage of norway spruce under high temperature. Fire Technol 57(5):2451–2490. https://doi.org/10.1007/s10694-021-01123-z
36. McGrattan K, McDermott R, Floyd J, Hostikka S, Forney G, Baum H (2012) Computational fluid dynamics modelling of fire. Int J Comput Fluid Dyn 26(6–8):349–361. https://doi.org/10.1080/10618562.2012.659663
37. McGrattan K, Hostikka S, Floyd J, McDermott R, Vanella M (2021) Fire dynamics simulator technical reference guide volume 1: mathematical model, revision: FDS6.7.7-0-gfe0d4ef38. National Institute of Standards and Technology, Gaithersburg
38. Arnold L, Hehnen T, Lauer P, Trettin C, Vinayak A (2018) PROPTI: a generalised inverse modelling framework. J Phys Conf Ser 1107(3):032016. https://doi.org/10.1088/1742-6596/1107/3/032016
39. Houska T, Kraft P, Chamorro-Chavez A, Breuer L (2015) SPOTting model parameters using a ready-made python package. PLoS ONE 10(12):e0145180. https://doi.org/10.1371/journal.pone.0145180
40. Dupal O, Hasalová L, Šálek V, Hejtmánek P, Jahoda M (2022) Use of photogrammetry to determine spruce and OSB char bulk density. Fire Mater . https://doi.org/10.1002/fam.3113

41. Chaos M (2014) Spectral aspects of bench-scale flammability testing: application to hardwood pyrolysis. In: Spearpoint M (ed) Fire safety science – Proceedings of the Eleventh International Symposium. International Association for Fire Safety Science, London, pp 165–178. https://doi.org/10.3801/IAFSS.FSS.11-165
42. Ryder N, Weckman E (2013) Effects of convective heat transfer coefficient in prediction of materials properties from cone calorimeter testing. In: Babrauskas V, Grayson S, Hirschler M, Janssens M, van Hees P (eds) Fire and Materials 2013 – 13th international conference and exhibition, conference proceedings. Interscience Communications, London, pp 379-388
43. Fredlund B (1988) A Model for heat and mass transfer in timber structures during fire: a theoretical, numerical and experimental study. Dissertation, Lund University
44. Alves SS, Figueiredo JL (1989) A model for pyrolysis of wet wood. Chem Eng Sci 44(12):2861–2869. https://doi.org/10.1016/0009-2509(89)85096-1
45. Anca-Couce A, Zobel N, Berger A, Behrendt F (2012) Smouldering of pine wood: kinetics and reaction heats. Combust Flame 159(4):1708–1719. https://doi.org/10.1016/j.combustflame.2011.11.015
46. Ding Y, Wang C, Lu S (2015) Modeling the pyrolysis of wet wood using FireFOAM. Energy Convers Manag 98:500–506. https://doi.org/10.1016/j.enconman.2015.03.106
47. McGrattan K, Hostikka S, Floyd J, McDermott R, Vanella M (2021) Fire dynamics simulator user's guide, revision: FDS6.7.7-0-gfe0d4ef38. National Institute of Standards and Technology, Gaithersburg
48. Korhonen T, Hakkarainen T, Tissari A, Korkealaakso A, Kling T, Verma N (2021) Kartiokalorimetrikokeen mallitus FDS-ohjelmalla. In: Palotutkimuksen päivät 2021. Palotutkimusraati, Helsinki, pp 72–76
49. Korhonen T, Korkealaakso A, Verma N, Kling T, Hakkarainen T, Viitanen A (2022) Fast cone calorimeter model for optimization of pyrolysis parameters. In: Dederichs A (ed) et alNordic fire and safety days 2022: Book of abstracts RISE Research Institutes of Sweden, Gothenburg, pp 30–31
50. Li K, Pau DSW, Wang J, Ji J (2015) Modelling pyrolysis of charring materials: determining flame heat flux using bench-scale experiments of medium density fibreboard (MDF). Chem Eng Sci 123:39–48. https://doi.org/10.1016/j.ces.2014.10.043
51. McGrattan K, Hostikka S, Floyd J, McDermott R, Vanella M (2022) Fire dynamics simulator technical reference guide volume 3: validation, revision: FDS6.7.9-0-gec52-dee42. National Institute of Standards and Technology, Gaithersburg
52. König J, Walleij L (1999) One-dimensional charring of timber exposed to standard and parametric fires in initially unprotected and postprotection situations. Trätek, Stockholm
53. VTT Expert Services (2016) One-dimensional charring of solid timber, glued-laminated timber, LVL and CLT, Test report VTT-S-04746-16. VTT Expert Services, Espoo
54. Lautenberger C, Fernandez-Pello C (2009) Generalized pyrolysis model for combustible solids. Fire Saf J 44(6):819–839. https://doi.org/10.1016/j.firesaf.2009.03.011